Capacity Approaching Codes for the Non-Coherent FSK Channel

Albert Guillén i Fàbregas and Alex Grant
Institute for Telecommunications Research
University of South Australia
Mawson Lakes SA 5095, Australia
albert.guillen@unisa.edu.au, alex.grant@unisa.edu.au

***Abstract*— This paper describes a curve-fitting approach for the design of capacity approaching coded modulation for orthogonal signal sets with non-coherent detection. In particular, bit-interleaved coded modulation with iterative decoding is considered. Decoder metrics are developed that do not require the knowledge of the signal-to-noise ratio, yet still offer very good performance.**

I. Introduction

Orthogonal modulation with non-coherent detection is a practical choice for situations where the received signal phase cannot be reliably estimated and/or tracked. There are many important applications where this is the case. Examples include military communications using fast frequency hopping, airborne communications with high Doppler shifts due to significant relative motion of the transmitter and receiver, and high phase noise scenarios, due to the use of inexpensive or unreliable local oscillators.

A common choice of implementation for the modulator is frequency shift keying (FSK), and in the remainder of the paper we will therefore refer to non-coherent FSK (NC-FSK).

Capacity analysis of M-ary NC-FSK [1] reveals a trade-off between the modulation order M and the minimum energy per bit E_{b} required for reliable communications. Increasing M reduces the required E_{b}. This is useful in cases where transmit power is more important than spectral efficiency, such as low probability of intercept communications.

It is therefore of some interest to consider the design of error control codes which approach the capacity of these non-coherent channels. In the literature, concatenations of Reed Solomon (RS) codes and convolutional codes have been considered [2], as well as RS codes combined with repeat diversity [3], [4], [5]. Trellis coded modulation has been considered in [6]. The use of turbo codes has been considered in [7], [8], where the capacity of the binary NC-FSK channel was approached within about 0.7 dB on Rayleigh fading channels. As discussed above however, higher order modulation may be of more interest.

More recently, bit interleaved coded modulation with iterative decoding (BICM-ID) [9], [10] has been considered for the NC-FSK channel [11], [12], [13]. Using the standard cdma2000 turbo code with rates $1/2$, $1/3$, $1/4$ and $1/5$ they report simulation results ranging from about 0.9 dB from capacity for 4-ary NC-FSK to about 1.7 dB from capacity for 64-ary NC-FSK (with Rayleigh fading). Although a gain is demonstrated by iterating between demodulation and decoding, no optimization of the component codes is considered.

Another important consideration in many applications is the amount of channel state information (CSI) available at the decoder. This may range from full CSI, where the decoder knows the instantaneous fading amplitude and the average signal-to-noise ratio (SNR), to partial CSI, where only the average SNR is known, right through to no CSI, where not even the SNR is known. The latter case is of interest for partial band jamming of a fast frequency hopped system, where the resulting SNRs for each of the M frequency bins may vary with frequency and time. Valenti and Cheng [13] develop decoder metrics for both the full and partial CSI scenarios, but do not consider the complete absence of CSI.

There are two main contributions in this paper. First, in Section III, we develop low-complexity decoder metrics suitable for iterative decoding/demodulation with no CSI. We demonstrate the corresponding effect of loss of CSI on the extrinsic information (EXIT) charts [14] of the demodulator. Secondly, in Section IV we use curve fitting of EXIT charts [15], [16] to optimize the degree sequences for outer irregular repeat-accumulate codes [17] for use with a an inner rate-1 recursive M-ary modulator. The resulting codes outperform all previously reported results for the NC-FSK channel.

Notation: All vectors will be column vectors, and will be denoted using bold face, e.g. $\mathbf{x} = (x_1, x_2, \ldots, x_n)^t \in \mathbb{C}^n$ is a column vector with n complex elements. $\mathcal{N}\left(\mu, \sigma^2\right)$ denotes the circularly symmetric complex Gaussian density, with mean μ and variance $\sigma^2/2$ in the real and imaginary components. $|\cdot|$ denotes the magnitude of its complex argument.

II. System Model

We assume that the modulation order is a power of two, $M = 2^m$. With reference to Figure 1, an information source produces a binary sequence $u[i]$, $i = 0, 1, \ldots, RLm-1$, which is encoded at rate R to produce the binary sequence $c[j]$, $j = 0, 1, \ldots, Lm-1$. The coded bit sequence is bit-wise permuted, resulting in $c[\pi(j)]$.

The output of the M-FSK modulator is a sequence of M-vectors $\mathbf{x}[k]$, $k = 0, 1, \ldots, L-1$. Each element $x_b[k]$ of this vector corresponds to one of the M frequency bins. Hence each vector $\mathbf{x}[k]$ is all zeros, except for a single element $x_b[k] = 1$, corresponding to transmission on a particular frequency bin

[1]This work has been supported by the Australian Research Council (ARC) Grants DP0344856 and DP0558861.

$b \in \{0, 1, \ldots, M-1\}$ at time k. The output alphabet of the modulator is therefore $\mathcal{E} = \{\mathbf{e}_b : b = 0, 2, \ldots, M-1\}$, where $\mathbf{e}_b$ is the canonical basis vector with a one at position b and zeros everywhere else.

For the moment we leave the precise modulation mapping unspecified. A memoryless modulator performs a natural mapping of consecutive blocks of m bits from $c[j]$. Alternatively, the modulator could have memory (e.g. a rate 1 recursive trellis code).

The channel output at symbol time k is given by

$$\mathbf{y}[k] = \sqrt{E_\mathrm{s}} h[k] \mathbf{x}[k] + \mathbf{n}[k]$$

where E_s is the per-symbol transmit power, $h[k] \in \mathbb{C}$ is the channel gain at time k and $\mathbf{n}[k] \sim \mathcal{N}(0, N_0)$ is a vector of zero-mean circularly symmetric complex Gaussian noise samples, with variance N_0.

Setting $h[k] = 1$ for $k = 0, 1, \ldots, L-1$, results in an additive white Gaussian noise (AWGN) channel. Fast, flat fading is modeled by letting $h[k] \sim \mathcal{N}(0, 1)$, or in polar coordinates, $h[k] = a[k] e^{i\theta[k]}$ with $a[k]$ i.i.d. Rayleigh and $\theta[k]$ uniform over $[0, 2\pi)$. Thus under either channel model, the average SNR is $\gamma \triangleq E_\mathrm{s}/N_0$, while for the Rayleigh channel, the instantaneous SNR is $a^2[k]\,\gamma$. The energy per source bit is $E_\mathrm{b} = E_\mathrm{s}/(Rm)$.

Where it causes no confusion, we will omit the symbol time indexing k.

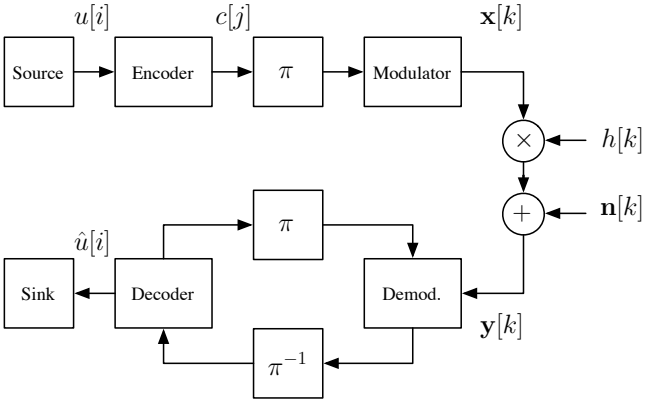

Fig. 1. System model.

A non-coherent receiver simply measures the energy $|y_b|^2$ of each frequency bin, and the resulting channel transition probabilities are given by [18]

$$p(\mathbf{y} \mid \mathbf{x} = \mathbf{e}_b) = K I_0\left(2\frac{\sqrt{E_\mathrm{s}}}{N_0} a |y_b|\right) \qquad (1)$$

where the normalization constant

$$K = \left(\frac{\gamma}{\pi}\right)^M e^{-\gamma\left(a^2 + \|\mathbf{y}\|^2\right)}$$

is independent of the hypothesis b, and $I_0(.)$ is the 0-th order modified Bessel function of the first kind [19]. Note that the transition probabilities depend on the ratio $a\sqrt{E_\mathrm{s}}/N_0$ rather than the ratio $a^2\,\gamma$ appearing in coherent detection.

The transition probabilities in (1) can be very easily evaluated with extremely high precision and low-complexity using with the algorithm presented in [20] based on the polynomial expansions of [19].

The capacity of the non-coherent FSK channel was found by Stark in [1]. Figure 2 shows the minimum E_b/N_0 (in dB) required for reliable communication with M-FSK with non-coherent detection in AWGN, for $M = 2, 4, 8$. The coherent BPSK AWGN channel is shown for comparison (dashed line).

There are two main observations. First, increasing the bandwidth (increasing M) reduces the required E_b/N_0. Secondly, in contrast to the coherent channel, as the code rate $R \to 0$, the required $E_\mathrm{b}/N_0 \to \infty$. Thus there is a non-trivial rate which optimizes the required E_b/N_0 for any given M.

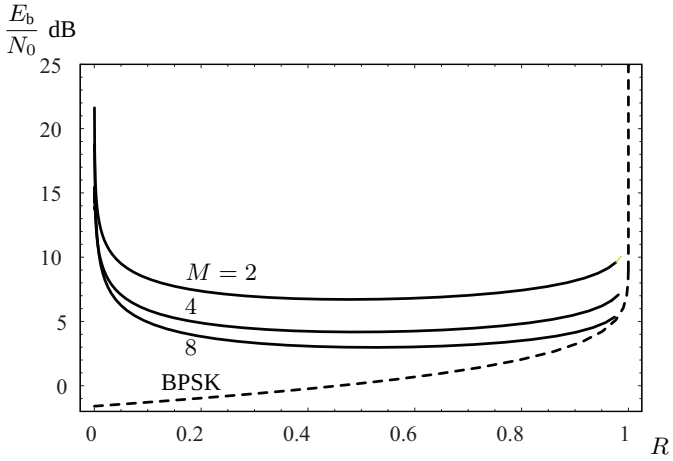

Fig. 2. Minimum E_b/N_0 versus code rate R required for reliable communication with M-ary FSK with non-coherent detection in AWGN for $M = 2, 4, 8$.

III. Metrics for Iterative Decoding

Iterative decoding of BICM [9], [10] has shown promise for the NC-FSK channel [13]. The main idea is to iterate between soft demodulation and soft decoding, as shown in Figure 1. Gains of 0.7 to 1 dB have been reported compared to single-pass decoding of BICM.

In this section we will develop metrics suitable for use in such decoders. There are two main design objectives. First, the metrics should have a simple implementation. Secondly, it is desirable to develop metrics that do not require any CSI, i.e. do not depend on $a[k]$, E_s and N_0.

A memoryless NC-FSK modulator transmits $\mathbf{x}[k] = \mathbf{e}_b$ at symbol time k where the active frequency bin b is according to

$$b = \sum_{i=0}^{m-1} c[j(k,i)]\, 2^i.$$

where $j(k,i) = \pi^{-1}(mk + i)$, $i = 0, 1, \ldots, M-1$ are the indexes of the m coded bits modulated into symbol k.

Let $\mathcal{B}_0^i = \{b \in \{0, 1, \ldots, M-1\} : b \wedge 2^i = 0\}$ and $\mathcal{B}_1^i = \{b \in \{0, 1, \ldots, M-1\} : b \wedge 2^i = 1\}$, where $\wedge$ denotes the bitwise AND operation. Thus $\mathcal{B}_0^i$ is the set of indexes with a zero in the i-th position of their binary representation and $\mathcal{B}_1^i$ is the set with a one at that position.

For $b \in \{0, 1, \ldots, M-1\}$, $k \in \{1, 2, \ldots, L-1\}$ and $i \in \{0, 1, \ldots, m-1\}$, define the extrinsic probabilities [21]

$$q_{k,i}(b) = \prod_{\substack{l=0 \\ l \neq i}}^{m-1} \Pr\left(c[j(k,l)] = 2^l \wedge b\right).$$

Standard iterative BICM demodulation [9] consists of feeding the decoder with the following metrics (in log-likelihood ratio form)

$$\begin{aligned}\mathcal{L}(c[j(k,i)]) &= \log \frac{p(c[j(k,i)]=0)}{p(c[j(k,i)]=1)} \\ &= \log \frac{\sum_{b\in\mathcal{B}_0^i} p\left(\mathbf{y}[k] \mid \mathbf{e}_b\right) q_{k,i}(b)}{\sum_{b\in\mathcal{B}_1^i} p\left(\mathbf{y}[k] \mid \mathbf{e}_b\right) q_{k,i}(b)}. \end{aligned} \quad (2)$$

Substituting (1) into (2), we obtain the iterative decoder used by [13].

The summations in (2) may be undesirable from the point of view of complexity. To avoid these summations, the log likelihood ratio (2) may be approximated in the following standard way

$$\begin{aligned}\mathcal{L}(c[j(k,i)]) \approx & \max_{b\in\mathcal{B}_0^i} \log I_0\left(2\frac{\sqrt{E_\mathrm{s}}}{N_0}a[k]\,|y_b[k]|\right) q_{k,i}(b) \\ & - \max_{b\in\mathcal{B}_1^i} \log I_0\left(2\frac{\sqrt{E_\mathrm{s}}}{N_0}a[k]\,|y_b[k]|\right) q_{k,i}(b) \end{aligned} \quad (3)$$

We shall refer to (2) and (3) as the Bessel and Bessel dual-max metrics respectively.

Note that in order to compute (2) and (3), the signal energy, the noise variance and the fading coefficients (or sufficiently accurate estimates) must be available to the receiver. Both of these metrics require full CSI.

A. Parameter Free Metrics

We will now develop decoder metrics that do not depend on E_s, N_0 or $a[k]$. Taylor series expansion of the Bessel function $I_0(\alpha)$ around zero yields

$$I_0(\alpha) = 1 + \frac{\alpha^2}{4} + O(\alpha^4) \quad (4)$$

which motivates the following approximation of the log-likelihood ratios (2),

$$\mathcal{L}(c[j(k,i)]) \approx \log \frac{\frac{M}{2} + \frac{E_\mathrm{s}}{N_0^2}a[k]^2 \sum_{b\in\mathcal{B}_0^i} |y_b[k]|^2 q_{k,i}(b)}{\frac{M}{2} + \frac{E_\mathrm{s}}{N_0^2}a[k]^2 \sum_{b\in\mathcal{B}_1^i} |y_b[k]|^2 q_{k,i}(b)}. \quad (5)$$

If we further assume that

$$\frac{E_\mathrm{s}}{N_0^2}a[k]^2 \sum_{b\in\mathcal{B}_0^i} |y_b[k]|^2 \gg M/2 \quad (6)$$

we have

$$\mathcal{L}(c[j(k,i)]) \approx \log \frac{\sum_{b\in\mathcal{B}_0^i} |y_b[k]|^2 q_{k,i}(b)}{\sum_{b\in\mathcal{B}_1^i} |y_b[k]|^2 q_{k,i}(b)} \quad (7)$$

which is independent of E_s, N_0 and the fading amplitudes $a[k]$.

The interpretation of (7) is interesting. The receiver first measures the received energies at every frequency bin and computes the *empirical probability* at every bin as the fraction of the total received energy present in a given bin. Obviously, the normalization factor (the total energy $\sum_{i=0}^{M-1} |y_b[k]|^2$) simplifies in (7).

We can further approximate (7) using the dual-max method as follows,

$$\begin{aligned}&\mathcal{L}(c[j(k,i)]) \approx \\ &\quad \max_{b\in\mathcal{B}_0^i} \log(|y_b[k]|^2 q_{k,i}(b)) - \max_{b\in\mathcal{B}_1^i} \log(|y_b[k]|^2 q_{k,i}(b)) \end{aligned} \quad (8)$$

which yields the corresponding parameter free dual-max metrics.

B. Numerical Examples

Before proceeding further, we present some numerical examples which demonstrate the utility of the parameter free metrics. Since we are interested in application of the metrics to iterative decoding, it is of interest to compare the corresponding EXIT charts [22].

Figure 3 shows EXIT charts for soft demodulation using the Bessel metrics (2) (solid), dual-max Bessel (3) (dashed), and the parameter free metrics (7) (dashed-dotted) and (8) (dotted). The charts are for 4-FSK, 16-FSK and 64-FSK modulation on the AWGN channel, Figure 3(a) and on the Rayleigh fading channel, Figure 3(b).

The first observation is that the curves exhibit an almost-linear behavior, with Bessel metrics and parameter free metrics resulting in similar slopes. This implies that at higher γ, the parameter metrics will have the same EXIT chart, which will help in assessing the performance degradation due to the lack of CSI.

Further, we observe that the parameter free metrics are information lossy, namely, when the input mutual information is $I_\mathrm{in} = 1$, the output mutual information is lower than that obtained with Bessel metrics.

Finally, and perhaps most surprising, the parameter free dual-max metric (8) is significantly better than (7) at low I_in, despite the reduction in computational complexity. Application of the dual-max approximation following the Taylor approximation seems to regain some of the loss from the ideal Bessel metrics.

Figure 4(a) shows the demodulator EXIT charts for metrics (2), (7) and (8) at their respective SNR thresholds with the $(25, 27, 33, 37)_8$ convolutional code. Figure 4(b) shows the corresponding BER simulations with 10 decoding iterations and 10000 information bits per codeword. For the sake of clarity, we do not show the curves for the Bessel dual-max metrics (3), as the results are only slightly worse than the standard Bessel metrics (2).

The EXIT analysis predicts the threshold behavior quite accurately for (2) and (8). From Figure 4(b), it is apparent that as M grows, the error floor is pushed down to lower error rates, effectively disappearing for 64-FSK at BERs of practical interest.

We also see that the metric (7) exhibits significant performance degradation with respect to its simpler dual max counterpart (8). The self-normalized dual-max metrics (8) prove to be very robust and show performance close to the ideal

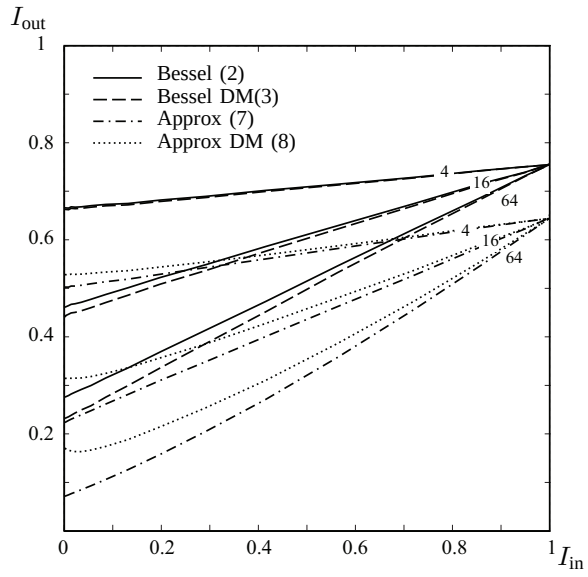

(a) AWGN

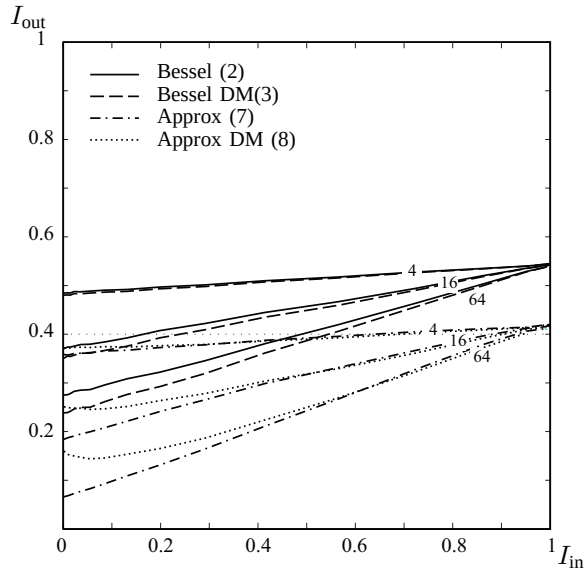

(b) Rayleigh Fading

Fig. 3. EXIT charts of the Bessel and parameter free metrics for 4, 16 and 64 NC-FSK on the AWGN (a) and Rayleigh fading (b) channel with $\gamma = 6$ dB.

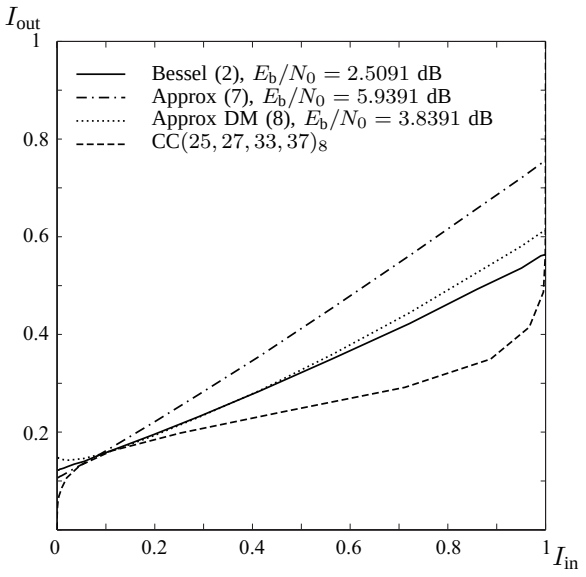

(a) EXIT charts for 64-ary NC-FSK. Each demodulator chart is shown at its E_{b}/N_0 threshold.

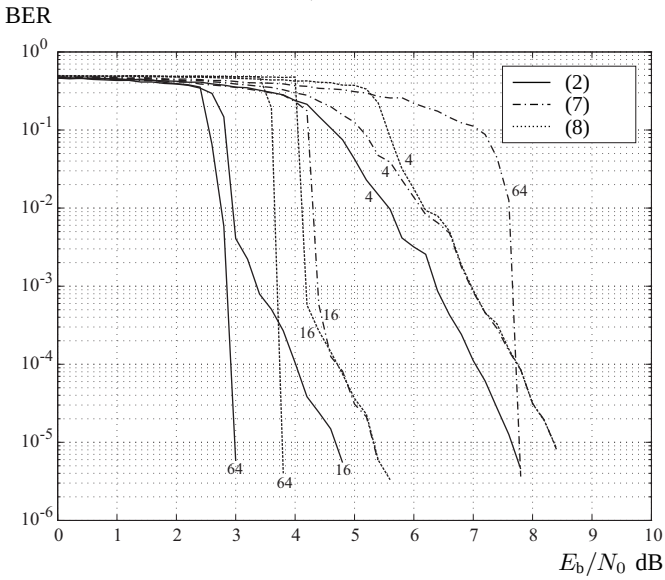

(b) Simulated BER results for 4, 16 and 64-ary NC-FSK.

Fig. 4. EXIT chart and BER results for BICM over the AWGN channel with a $(25, 27, 33, 37)_8$ outer convolutional code using Bessel (2) and parameter free metrics (7), (8).

Bessel metric. This result is quite remarkable, as the loss for not knowing the γ is shown to be around 0.6 dB.

Figure 5 shows the simulated bit-error rate for BICM with an outer rate $R = 1/2$ repeat-accumulate code and 4, 16 and 64-ary NC-FSK. Figure 5(a) is for AWGN only, while Figure 5(b) is for Rayleigh fading. Metrics (2), (7) and (8) are considered.

The simulations were performed using $10,000$ information bits per codeword and 20 decoding iterations (one iteration of the RA decoder per demodulation iteration). Once again, the metrics (7) offer poor performance as M grows. In this case, the dual-max metric (8) pays a maximum penalty of only about 1.5 dB for not knowing E_{s}, N_0 or the fading amplitude.

IV. Code Optimization

The results presented in the previous section were for BICM with an arbitrary selection of outer code (a similar approach was taken in [13], where an off-the-shelf code was considered). Our main intention however was to evaluate the utility of the parameter free metrics. In this section we proceed to optimize the choice of outer code, and consider more suitable modulation mappings.

Motivated by the serially concatenated coded modulation (SCCM) scheme of Tüchler [23], we particularize it to M-ary orthogonal modulation with outer irregular repetition codes. This approach consists of concatenating a binary outer code with a jointly designed inner code and modulator through a bit interleaver π. So we still have the system of Figure 1,

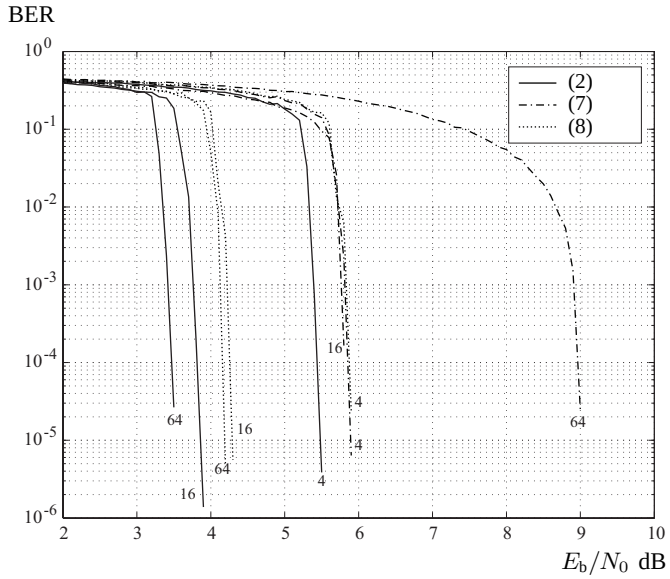

(a) AWGN channel.

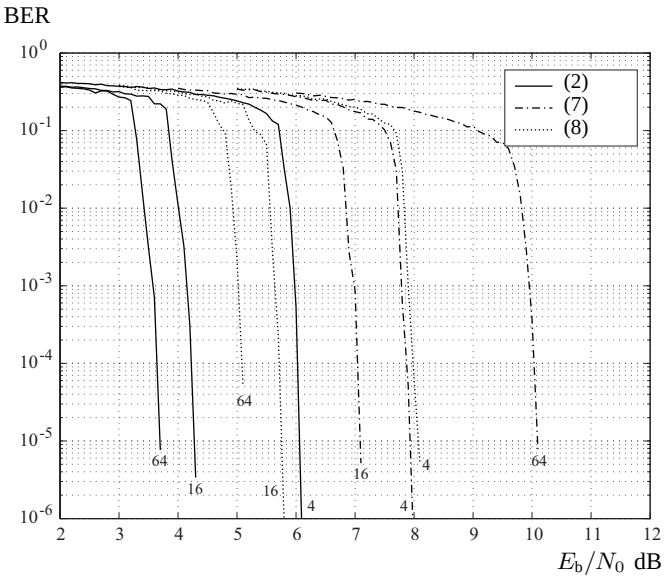

(b) Rayleigh fading channel.

Fig. 5. BER performance of BICM with outer rate $R = 1/4$ repeat accumulate code and 4, 16, 64 NC-FSK over AWGN and Rayleigh fading channel.

where rather than use a memoryless modulator, we use a coded modulator with memory.

With reference to Figure 6, we propose an inner encoder/modulator that operates as follows. Encoding is performed on blocks of $2m$ bits. Pairs of bits from the block of $2m$ bits undergo a single parity check. The result is then encoded by a recursive rate m/m trellis code. The output of the recursive encoder is finally fed to the standard M-ary NC-FSK memoryless modulator (described above in Section III). Thus the overall rate of the inner encoder/modulator is $2m$ bits per symbol.

Note that no interleaver is used between the encoder and the NC-FSK modulator, as suggested by [23]. An interesting characteristic of this inner code is that it reaches the $(1, 1)$ point on the EXIT chart [23]. The use of the single parity checks prior to trellis encoding further improves the properties of the resulting EXIT charts, as discussed in [15]. The particular choice of trellis code shown in Figure 6 has been hand-selected for properties that are particularly convenient when it comes to optimizing the outer code.

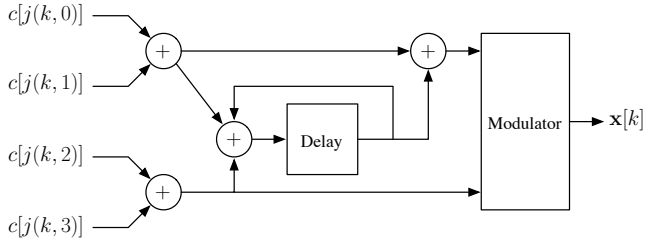

(a) 4 NC-FSK

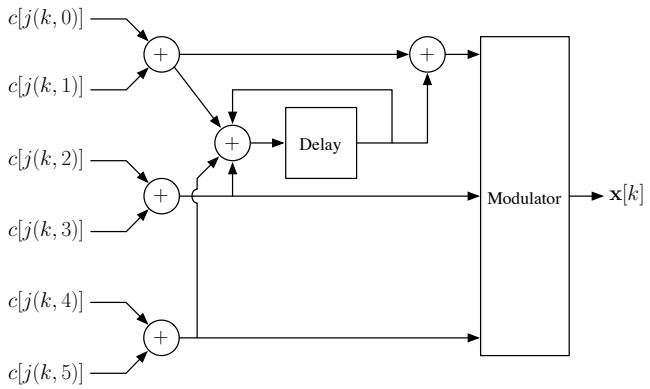

(b) 8 NC-FSK

Fig. 6. Inner encoder/modulator for 4 and 8-ary NC-FSK.

For the outer code, we will use an irregular non-systematic repetition code of length n, defined by the degree distribution (edge perspective)

$$\left\{ \lambda_i \geq 0, i = 2, \ldots, d_{\max} : \sum_{i=2}^{d_{\max}} \lambda_i = 1 \right\},$$

where λ_i is the fraction of edges in the outer code graph connected to information bit nodes of degree i, and $d_{\max}$ is the maximum allowed degree (see [24] for details).

With these definitions, the number[2] of information bit nodes of degree i of the outer code is given by $k_i = \lambda_i n/i$ and the resulting code rate is

$$R = \frac{1}{n} \sum_{i=2}^{d_{\max}} k_i = \sum_{i=2}^{d_{\max}} \frac{\lambda_i}{i}.$$

The factor graph representation [25] of the overall serially concatenated code is shown in Figure 7. In our design, we do not use grouping nodes [24]. In a sense, the inner code nodes act as grouping nodes of grouping factor $2m$.

[2]In practice, some small adjustments are required to ensure that the k_i are integer.

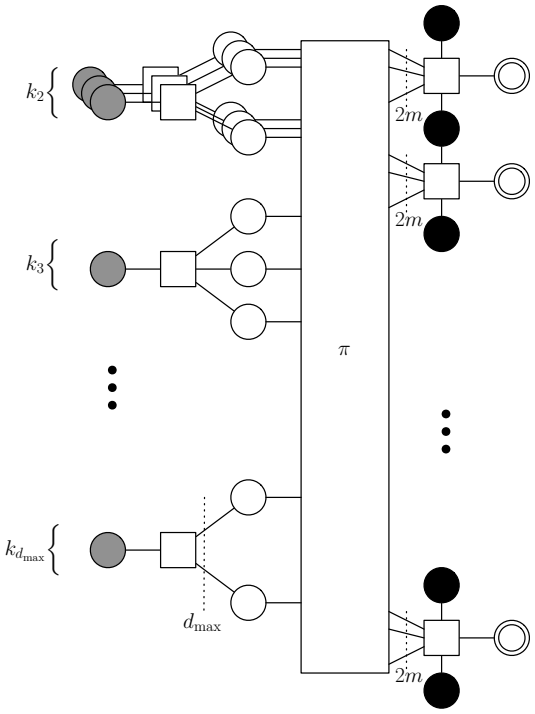

Fig. 7. Factor graph representation of the entire code. Grey circles denote the message bits, the white circles denote the outer coded bits, double circles denote the M-ary symbols, black circles represent the inner code state. Squares represent the encoding constraint functions.

As shown in [14] for the binary erasure channel, the gap between capacity and the decoding threshold for iteratively decoded codes is related to the area between the EXIT charts of the outer and inner codes. This idea has been extensively used to optimize various irregular code ensembles over the AWGN [23], [15], [24]. In the AWGN channel, the area theorem [14] is not exact. For exact results the reader is referred to the generalized EXIT charts of [26]. Unfortunately, computing these generalized charts is not a simple task. However, codes resulting from optimization with standard EXIT charts are usually as close as desired from capacity (see e.g. [23], [15], [24]).

Let $I^I(u,\gamma)$ be the EXIT chart of the inner code at a given SNR γ and a priori mutual information u. Let $I_i^O(u)$ denote the EXIT chart of an outer regular repetition code of degree i. We can easily evaluate I_i^O in terms of the well-known J function [15] as follows,

$$I_i^O = J\left(J^{-1}(u)\sqrt{i-1}\right), \quad \text{where}$$

$$J(x) = 1 - \int \frac{e^{-(t-x^2/2)}/2x^2}{\sqrt{2\pi x^2}} \log_2(1+e^{-t})dt$$

Accurate numerical evaluation is possible using the approximations in [16].

Finally, the EXIT chart of an irregular repetition code is simply the weighted sum of the degree-i charts [14], [15], [16]

$$I^O = \sum_{i=1}^{d_{\max}} \lambda_i I_i^O.$$

We can therefore use linear programming to optimize the outer code degree distribution, to minimize the area between the inner and outer code EXIT charts.

Figure 8 shows the results of this curve fitting procedure for 4 and 8-ary modulation with rate $1/2$ codes. Degree distributions, and thresholds for these codes, as well as rate $1/4$ are shown in Table I. The thresholds are given in terms of the distance to capacity Δ_C dB.

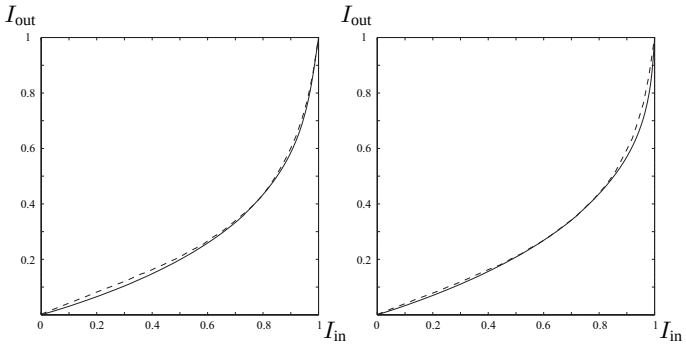

(a) 4 NC-FSK at $E_{\text{b}}/N_0 = 4.35$ dB.

(b) 8 NC-FSK at $E_{\text{b}}/N_0 = 3.039$ dB.

Fig. 8. EXIT charts of optimized 4 and 8-ary NC-FSK coded modulation. Solid line is the outer code. Dashed line is the inner coded modulator

Figure 9 shows simulated BER results for the optimized rate $1/2$ codes with 4 and 8 NC-FSK the AWGN channel, along with capacity (solid) and the predicted decoding threshold (dashed). A block length of $100,000$ was used for the simulation with 100 decoding iterations. These results clearly validate the code design using curve fitting of EXIT charts.

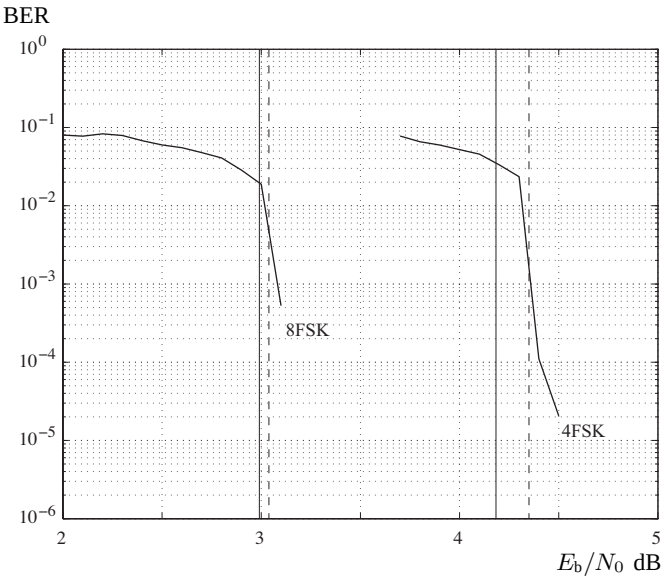

Fig. 9. Simulated BER results for the optimized codes on the AWGN channel.

Table I summarizes the results of our code design. There are two main conclusions. First, we have found codes very close to capacity, ranging from 0.17 - 0.05 dB. This can be compared to gaps of 0.9 - 1.7 dB reported in [13], where no code optimization was performed. Secondly, the maximum degree for the optimized codes is not unrealistically high. In our linear program we allowed much higher $d_{\max}$ (up to 50), but fortuitously such high degree nodes were not required. These low maximum degrees, coupled with the extremely simple inner code results in a system with very low implementation complexity.

TABLE I
OPTIMAL CODES FOR $M = 4, 8, 16$ AND 64 IN THE AWGN CHANNEL WITH BESSEL MATRICS.

M	R	Capacity	Threshold	Distribution
4	1/4	4.6172 dB	4.7602 dB	$\lambda_2 = 0.0483$ $\lambda_4 = 0.1250$ $\lambda_{11} = 0.0911$ $\lambda_{12} = 0.7356$
	1/2	4.1809 dB	4.3500 dB	$\lambda_2 = 0.1413$ $\lambda_4 = 0.1523$ $\lambda_5 = 0.7064$
8	1/4	3.5484 dB	3.5994 dB	$\lambda_2 = 0.0193$ $\lambda_4 = 0.0193$ $\lambda_{10} = 0.8655$
	1/2	2.9904 dB	3.0391 dB	$\lambda_2 = 0.0581$ $\lambda_4 = 0.6512$ $\lambda_5 = 0.2907$
16	1/4	2.5921 dB	2.600 dB	$\lambda_2 = 0.042017$ $\lambda_4 = 0.0442165$ $\lambda_5 = 0.151857$ $\lambda_{12} = 0.617372$ $\lambda_{13} = 0.1445366$
	1/2	2.0685 dB	2.1397 dB	$\lambda_2 = 0.128628$ $\lambda_4 = 0.255314$ $\lambda_5 = 0.575429$ $\lambda_6 = 0.040627$
64	1/4	1.6845 dB	1.6890 dB	$\lambda_2 = 0.04975$ $\lambda_6 = 0.163822$ $\lambda_7 = 0.425504$ $\lambda_{30} = 0.36091$
	1/2	1.1155 dB	1.1487 dB	$\lambda_2 = 0.114061$ $\lambda_3 = 0.156532$ $\lambda_4 = 0.463261$ $\lambda_{10} = 0.085959$ $\lambda_{11} = 0.180176$

V. CONCLUSIONS

We have found a low complexity method of computing metrics suited for iterative demodulation/decoding of M-ary non-coherent orthogonal modulation that does not require any knowledge of the signal-to-noise ratio or fading coefficients at the receiver. The method is based on the first-order Taylor series expansion of the Bessel function. The proposed method performs within 0.6 dB of the ideal metrics. This enables the use of methods such as bit-interleaved coded modulation over non-coherent channels without side information.

We have also designed new codes for the 4 and 8-ary non-coherent orthogonal modulation channel. These codes are a concatenation of an irregular repeat code and an two-state trellis coded modulator. By optimizing the degree sequence of the outer code we have found codes with decoding thresholds within 0.15 dB of capacity, surpassing all previously known codes. Furthermore, the optimized codes are very low complexity, with low maximum degree. A forthcoming journal paper will report addition results no CSI metrics.

REFERENCES

[1] W. E. Stark, "Capacity and cutoff rate of noncoherent FSK with nonselective rician fading," *IEEE Trans. on Commun.*, vol. 33, pp. 1153–1159, Nov. 1985.

[2] C. D. Frank and M. B. Pursley, "Concetenated coding for frequency-hop spread-spectrum with partial-band interference," *IEEE Trans. Commun*, vol. 44, no. 3, pp. 377–387, Mar. 1996.

[3] S. Kim and W. E. Stark, "Performance limits of Reed-Solomon coded CDMA with orthogonal signaling in a Rayleigh-fading channel," *IEEE Trans. Commun*, vol. 46, pp. 1125–1134, Sept. 1998.

[4] M. Chu and W. E. Stark, "Asymptotic performance of a coded communication system with orthogonal signaling in partial band jamming," in *IEEE Military Communications Conference*, 1998, pp. 1003–1007.

[5] J. D. Choi, D.-S. Yoo, and W. E. Stark, "Performance limits of m-FSK with Reed-Solomon coding and diversity combining," *IEEE Trans. Commun*, vol. 50, no. 11, pp. 1787–1797, Nov. 2002.

[6] G. Garrabrant and J. Ehrenberg, "Trellis coded modulaiton applied to noncoherent detection of orthogonal signals," in *IEEE Military Communications Conference*, Oct. 1989, pp. 774–8.

[7] J. Vainappel, E. Hardy, and D Raphaeli, "Noncoherent turbo decoding," in *IEEE Global Communications Conf.*, San Antonio, US, Nov. 2001, pp. 952–6.

[8] A. Ramesh, A. Chockalingham, and L. B. Milstein, "Performance of noncoherent turbo detection on rayleigh fading channels," in *IEEE Global Communications Conf.*, San Antonio, USA, Nov. 2001, pp. 1193–1198.

[9] X. Li and J. A. Ritcey, "Trellis-coded modulation with bit interleaving and iterative decoding," *IEEE JSAC*, pp. 715–724, April 1999.

[10] G. Caire, G. Taricco, and E. Biglieri, "Bit-interleaved coded modulation," *IEEE Trans. on Inform. Theory*, vol. 44, no. 3, pp. 927–946, May 1998.

[11] Shi Cheng and M.C. Valenti, "Bit-interleaved turbo-coded noncoherent orthogonal modulation with iterative demodulation and decoding: capacity limits and convergence analysis," in *Thirty-Eighth Asilomar Conference on Signals, Systems and Computers*, Nov. 2004, pp. 2020–2024.

[12] M. C. Valenti, E. Hueffmeier, B. Bogusch, and J. Fryer, "Towards the capacity of noncoherent orthogonal modulation: BICM-ID for turbo coded NFSK," in *IEEE Military Communications Conference*, 2004, pp. 1549–1555.

[13] M. C. Valenti and S. Cheng, "Iterative demodulation and decoding of turbo-coded M-ary noncoherent orthogonal modulation," *IEEE J. Select. Areas Commun (Special Issue on Differential and Noncoherent Wireless Communications)*, vol. 23, no. 9, pp. 1739–1747, Sept. 2005.

[14] A. Ashikhmin, G. Kramer, and S. ten Brink, "Extrinsic information transfer functions: model and erasure channel properties," *IEEE Trans. Inform Theory*, vol. 50, no. 11, pp. 2657–2673, Nov. 2004.

[15] S. ten Brink and G. Kramer, "Design of repeat accumulate codes for iterative detection and decoding," *IEEE Trans. Sig. Proc.*, vol. 51, no. 11, pp. 2764–2772, Nov. 2003.

[16] S ten Brink, G. Kramer, and A. Ashikhmin, "Design of low-density parity-check codes for modulation and detection," *IEEE Trans. Commun*, vol. 52, no. 4, pp. 670–678, April 2004.

[17] H. Jin, A. Khandekar and R. McEliece, "Irregular repeat-accumulate codes," in *2nd International Symposium on Turbo Codes and Related Topics, Brest, France*, Sept. 2000.

[18] J. Proakis, *Digital Communications*, McGraw-Hill, 1995.

[19] M. Abramowitz and I. A. Stegun, *Handbook of Mathematical Functions with Formulas, Graphs and Mathematical Tables*, New York: Dover Press, 1972.

[20] W. H. Press, S. A. Teukolsky, W. T. Vetterling and B. P. Flannery, *Numerical Recepies in C*, Cambridge University Press, also available at `http://www.nr.com`, 1992.

[21] C. Berrou, A. Glavieux and P. Thitimajshima, "Near Shannon limit error correcting coding and decoding: Turbo codes," in *Proc. IEEE Int. Conference on Communications, Geneva, Switzerland*, 1993.

[22] S. ten Brink, "Designing iterative decoding schemes with the extrinsic information transfer chart," *AEU Int. J. Electron. Commun.*, vol. 54, no. 6, pp. 389–398, Dec. 2000.

[23] M. Tuechler, "Design of serially concatenated systems depending on the block length," *IEEE Trans. on Commun.*, vol. 52, no. 2, pp. 209–218, Feb. 2004.

[24] A. Roumy, S. Guemghar, G. Caire and S. Verdú, "Design methods for irregular repeat-accumulate codes," *IEEE Trans. Inform Theory*, vol. 50, no. 8, pp. 1711–1727, Aug. 2004.

[25] F. R. Kschischang, B. J. Frey, and H-A. Loeliger, "Factor graphs and the sum-product algorithm," *IEEE Trans. on Inform. Theory*, vol. 47, no. 2, pp. 498–519, Feb. 2001.

[26] A. Montanari C. Méasson and R. Urbanke, "Why we can not surpass capacity: the matching condition," *43rd Allerton Conference on Communication, Control and Computing*, Sept. 2005.